Structure of the signal recognition particle interacting with the elongation-arrested ribosome

Mario Halic[1], Thomas Becker[1], Martin R. Pool[2], Christian M. T. Spahn[3], Robert A. Grassucci[4], Joachim Frank[4] & Roland Beckmann[1]

[1]Institute of Biochemistry, Charité, University Medical School, Humboldt University of Berlin, Monbijoustrasse 2, 10117 Berlin, Germany
[2]University of Manchester, School of Biological Sciences, 2.205 Stopford Building, Oxford Road, Manchester M13 9PT, UK
[3]Institute of Medical Physics and Biophysics, Charité, University Medical School, Humboldt University of Berlin, Ziegelstrasse 9, 10117 Berlin, Germany
[4]Howard Hughes Medical Institute, Health Research Incorporated, Wadsworth Center, Empire State Plaza, Albany, New York 12201, and Department of Biomedical Sciences, State University of New York at Albany, Albany, New York 12222, USA

....

Cotranslational translocation of proteins across or into membranes is a vital process in all kingdoms of life. It requires that the translating ribosome be targeted to the membrane by the signal recognition particle (SRP), an evolutionarily conserved ribonucleoprotein particle. SRP recognizes signal sequences of nascent protein chains emerging from the ribosome. Subsequent binding of SRP leads to a pause in peptide elongation and to the ribosome docking to the membrane-bound SRP receptor. Here we present the structure of a targeting complex consisting of mammalian SRP bound to an active 80S ribosome carrying a signal sequence. This structure, solved to 12 Å by cryo-electron microscopy, enables us to generate a molecular model of SRP in its functional conformation. The model shows how the S domain of SRP contacts the large ribosomal subunit at the nascent chain exit site to bind the signal sequence, and that the Alu domain reaches into the elongation-factor-binding site of the ribosome, explaining its elongation arrest activity.

The existence of a signal sequence 'binding factor' for protein targeting to the endoplasmic reticulum was first proposed[1] in 1971. This binding factor was subsequently identified in a mammalian system as an 11S ribonucleoprotein (RNP) particle named the SRP[2]. This particle shows three main activities in the process of cotranslational targeting: first, it binds to signal sequences emerging from the translating ribosome; second, it pauses peptide elongation; and third, it promotes protein translocation by docking to the membrane-bound SRP receptor and transferring the ribosome nascent chain complex (RNC) to the protein-conducting channel[3].

These activities can be assigned to the two main domains of SRP that are separable by micrococcal nuclease treatment[4]. The first domain, the S domain, binds to signal sequences and promotes translocation[5]. It includes about half of the 7S RNA of SRP (roughly nucleotides 100–250), as well as the essential proteins SRP19, SRP54 and the SRP68–SRP72 (SRP68/72) heterodimer. Although SRP19 is required for SRP assembly[6], SRP54 is the functionally most significant protein subunit of the S domain: it recognizes the signal sequence[5] and interacts with the SRP receptor in a GTP-dependent manner[7]. SRP54 comprises an amino-terminal domain (N), a central GTPase domain (G) and a methionine-rich carboxy-terminal domain (M)[8], which anchors SRP54 to SRP RNA[9]. In addition, together with part of the RNA backbone[10], the M domain carries out the principal function of signal sequence recognition[11] near the peptide exit site of the large ribosomal subunit[12].

The second domain of SRP, the Alu domain, mediates the elongation arrest activity[13]. It is supposed to allow efficient targeting by providing a time window in which the nascent chain can be targeted to the translocation site[14–16]. The Alu domain contains the 5′ and 3′ parts of 7S RNA (including the *Alu*-like sequences), as well as the SRP9–SRP14 (SRP9/14) heterodimer, which is essential for its activity[17].

Little is known about the structural arrangement of the complete SRP[18,19], especially when bound to the active ribosome. How can SRP recognize a signal sequence and stop elongation at the same time? We have determined the structure of mammalian SRP bound to an elongation-arrested 80S ribosome bearing a nascent polypeptide chain containing a signal sequence at 12 Å resolution by using cryo-electron microscopy (cryo-EM) and single-particle reconstruction.

RNC purification and RNC–SRP reconstitution

Because the formation of a stable complex was a prerequisite for our study, we used wheat germ RNCs and canine SRP to reconstitute the targeting complex. This well-characterized combination, which led to the discovery of SRP, shows strong elongation arrest activity[14]. Assuming that this activity is a result of equally stable binding of the S and Alu domains to the ribosome, we considered that the wheat germ–canine heterologous complex was the most suitable candidate for structure determination.

We first isolated programmed ribosomes carrying a functional signal sequence (RNCs) from an *in vitro* translation reaction[20]. The nascent chain represented the first 90 amino acids of the type II membrane protein dipeptidylpeptidase B (DPAP-B) from yeast, which contains a signal anchor sequence, and also a haemagglutinin (HA) and histidine tag. Stalled RNCs were affinity purified and used for reconstitution with excess amounts of purified canine SRP (see Supplementary Information). To ensure specificity—that is, signal-sequence-dependent complex formation—we carried out sucrose density gradient centrifugation under high-salt conditions (500 mM potassium acetate)[21], which confirmed high-affinity binding of SRP to RNCs with an estimated occupancy of between 50 and 90% (see Supplementary Information).

Cryo-EM map and model of mammalian SRP

Cryo-EM and three-dimensional (3D) reconstruction of the targeting complex shows the typical appearance of an 80S ribosome at 12 Å resolution (7.7 Å according to the 3σ criterion; see Supplementary Information) with two additional densities (Fig. 1). First, a transfer RNA is visible in the P site in the ribosomal intersubunit space. Second, a large elongate mass representing SRP stretches from the peptide exit site of the 60S ribosomal subunit (S domain)
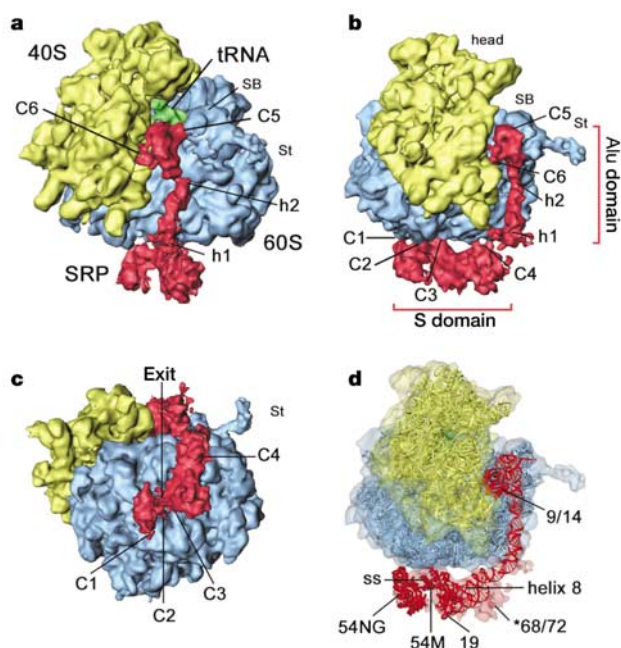
Figure 1 Cryo-EM map of mammalian SRP bound to 80S RNC at 12.0 Å. **a**, RNC–SRP map showing the separated colour-coded densities. The 40S small ribosomal subunit is shown in yellow, 60S large ribosomal subunit in blue, P-site tRNA in green, and SRP in red. C1–C6 indicate the assigned positions of RNC–SRP connections (see Table 1); h1 and h2 are hinges of the 7S RNA backbone of SRP; St, stalk; SB, stalk base. **b**, As **a**, but rotated by 70° to the right. **c**, As **a**, but rotated upwards by 90°. **d**, Same orientation as **b**, but with molecular models of SRP and 80S RNC shown in transparent densities.

RNC[20] (Figs 3 and 4) allowed the use of a previously generated molecular model[22]. Therefore, we use the yeast nomenclature for the molecular description of ribosomal components (with family names given in parentheses). For SRP we used X-ray structures of SRP fragments, which were docked into the density as rigid bodies (see Methods).

SRP has a bent conformation, with one of two hinges apparently facilitating a major kink (hinge 1) separating the S and Alu domains, in agreement with a three-domain structure of length 260–280 Å that has been proposed for SRP in solution[18]. Hinge 1 separates the 160-Å S domain of SRP near the peptide exit site from a linker connecting the Alu domain in a region close to the subunit interface (spanning a total length of 120 Å). The RNA at hinge 1 represents a large loop around nucleotides 100 and 250, and forms an angle of almost 90° (Figs 1b and 2). This site coincides precisely with the cutting site for micrococcal nuclease[4], which separates SRP into its main domains. Hinge 2 is located in a region corresponding to a small loop formed by nucleotides 70 and 275 of 7S RNA. This hinge facilitates a bend (∼ 30°) that leads to an orientation of the Alu 5′ RNP that is perfect for its entry into the intersubunit space (Figs 1a and 2f).

Into the density identified as the S domain, we docked the structure of a large fragment of the mammalian S domain containing 7S RNA helices 6–8 and part of helix 5, as well as the SRP19 protein and the SRP54 M domain[23]. The original SRP54 M domain was replaced with another model[24], which differs only in the position of helix 1 and the finger loop. As a signal sequence, we positioned an α-helical peptide fragment into the corresponding density near the exit site. As a result, it can contact the hydrophobic groove of the SRP54 M domain and the phosphate backbone of the SRP helix 8 RNA[10]. Next, we docked the conserved structure of a prokaryotic SRP54 NG domain[25]. Notably, the NG domain is positioned such that a gap of about 20 Å is separating it from helix 8 of 7S RNA, which is only connected by the M domain. In this position, part of the NG domain is too close to the finger loop of the M domain, indicating that there must be a more compact conformation of the loop for signal sequence binding. In support of our model, the crystal structure of an archaeal SRP54–RNA complex shows a similar overall arrangement[26].

We interpreted extra density in the S domain as the SRP68/72 dimer of a hitherto unknown structure. It is located mainly at the junction of helices 5–8; however, additional density is present at the hinge 1 region of helix 5 (Fig. 2c). This is in accordance with footprinting experiments showing that all of these regions of 7S RNA (including nucleotides 100 and 250) are protected[27]. The fragmented mass may be an indication of a tertiary structure

into the intersubunit space (Alu domain), forming a total of six connections (C1–C6) with the ribosome (Fig. 1).

The tRNA density reflects the presence of the nascent peptidyl-tRNA containing the signal sequence, which is stalled at the 3′ end of the truncated messenger RNA and stabilized by cycloheximide[20]. In agreement with the occupancy estimated by SDS polyacrylamide gel electrophoresis (SDS–PAGE), sorting the data set according to the presence of SRP density resulted in a subset of about 70% of the particles, which were used in the final reconstruction.

To facilitate interpretation on a molecular level, we attempted to dock molecular models into the electron densities (Fig. 2). For the ribosome, the high similarity between wheat germ RNC and yeast

Table 1 **Contacts between mammalian SRP and the 80S ribosome**

Contact	Type*	SRP	RNA/protein position	80S ribosome†	RNA/protein position‡
		S domain		60S subunit	
C1	p–p	54 NG	60–75	rpL25 (L23p)	130–135
	p–p	54 NG	15–26	rpL35 (L29p)	16–27
C2	p/R–p	54 M/H8	N terminus of M	Signal sequence	
	p–R	54 M	N terminus of M	H59/ES24	1,627–1,634§
C3	p–R	54 M	388–399	H24	490–495
C4	R–R/p	H5	218–228,121–127	H99, H100/101, rpL16	2,907–2,910, 2,849–2,851
	p–R/p	68/72		H98/ES39, rpL16 (L13p)	
		Alu domain		60S subunit	
C5	R–p	L1.2	135–136	rpL12 (L11p)	65–69
	R–R	L2	113	H43	1,171
	R–R	H2	109–119	H95/SRL	2,696–2,699
				40S subunit	
C6	p–R	14	74–89	h5, h15	55–58, 356–359; 368
	p–R	9	57–75	h5, h15	55–58, 368
	p–R	9	55–60	h14	341–344

*R and p correspond to RNA and protein, respectively.
†Yeast nomenclature is used with family name given in parentheses. ES, expansion segment.
‡Positions correspond to a model based on the yeast 80S ribosome[22].
§Positions correspond to yeast 25S RNA secondary structure (http://www.rna.icmb.utexas.edu/).

containing thin, extended 'tentacle' regions, as observed for some ribosomal proteins such as L19 or L22 (ref. 28). In the described position, SRP68/72 can function as a brace between the core of the S domain and the dynamic hinge 1, thereby functionally connecting the Alu and S domains.

The X-ray structure of the mammalian SRP9/14 dimer bound to the 5′ part of the Alu RNA[29] fits perfectly into the density in the intersubunit space (Fig. 2). This model matches a previously suggested conformation[29], in which the 5′ RNP, comprising the SRP9/14 dimer and the first 48 nucleotides of the RNA, folds back onto the 3′ RNA stem of the Alu domain. Thus, this back-folding seems to be a necessary assembly step of the Alu domain. In a final step, we used three fragments from a model provided by the SRP database[30] as a ruler to corroborate that the missing part of 7S RNA can span the distance between the docked Alu and S domain fragments.

Taken together, density consistent with size and structure could be assigned to all known components of the mammalian SRP, thereby leading to the first molecular model of SRP in the functional context of a ribosomal targeting complex.

An overview of the complete model in the context of the ribosome is shown in Figs 1d and 2e, f. The docked fragments easily span the distance between the peptide exit site and the binding site for elongation factors. The three connections of the S domain with the ribosome, found in the immediate vicinity of the peptide exit site, are contributed exclusively by the SRP54 protein. The Alu domain bridges, in a tight fit, the ~65 Å between the large and small ribosomal subunits (Fig. 2f). An empty space in the intersubunit
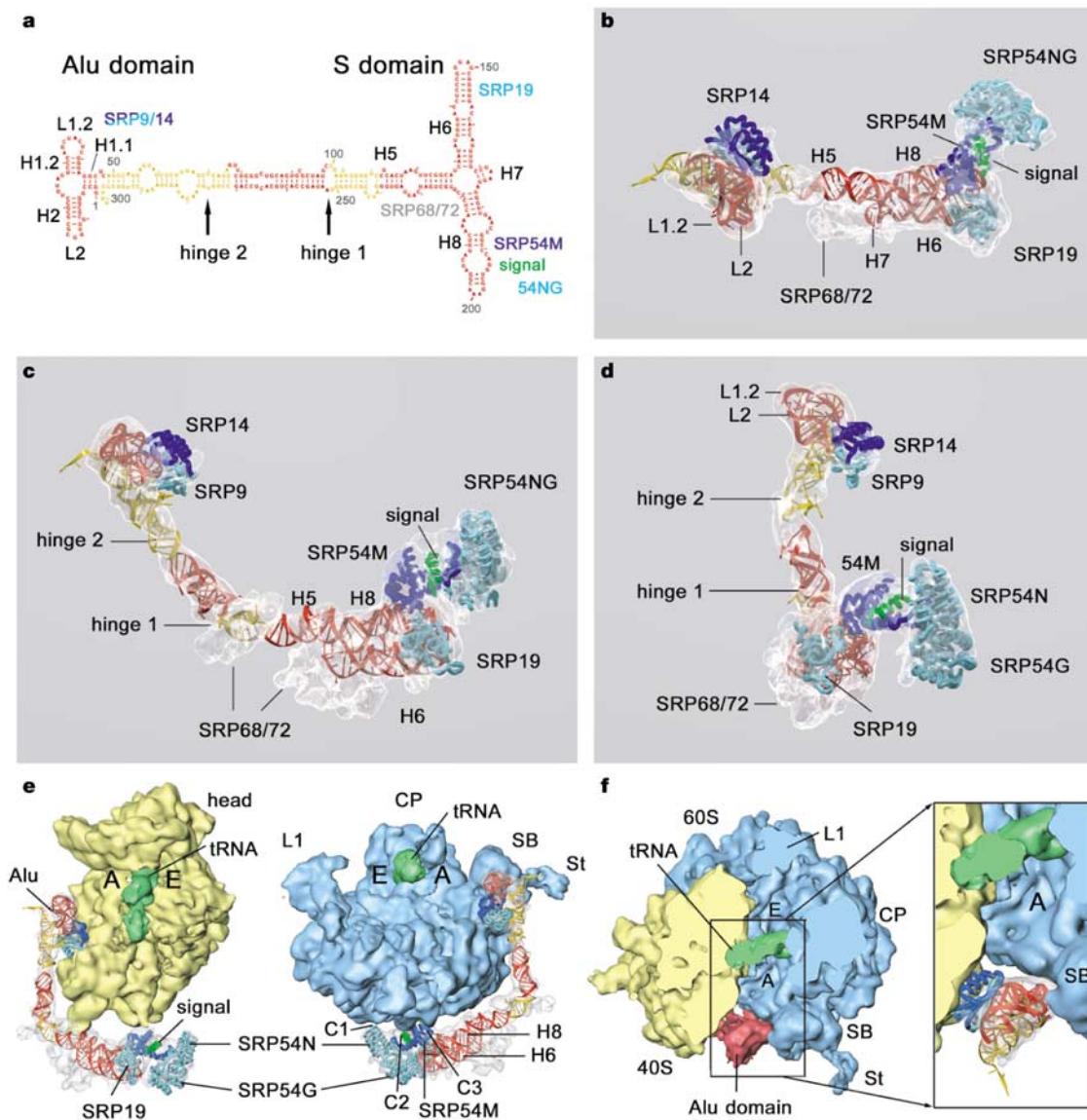
Figure 2 Molecular model of SRP. **a**, Secondary structure of SRP RNA with protein-binding sites and hinges indicated. H1–H8 denote SRP RNA helices, numbered according to ref. 29 for the Alu domain. SRP proteins are shown in cyan, blue and grey, 7S RNA in red and yellow, and the signal sequence in green. **b**, Molecular model of SRP with transparent density and colour coding as in **a**. Top view, SRP as seen from the ribosome. **c**, As **b**, but rotated upwards. **d**, As **c**, but rotated left. **e**, SRP with isolated 40S and 60S ribosomal subunits exposing the P-site tRNA (green), shown from the 60S (left) and the 40S (right) side. A and E, positions of the A and E sites; Alu, Alu domain; head, head of 40S subunit; L1, L1 protuberance; CP, central protuberance. Other labels are the same as in **a**. **f**, Cut top view showing the Alu domain in the intersubunit space (left), labelled as in **e**, and magnified view showing a molecular model of the Alu domain coloured as in **a**.

cavity, corresponding to the unoccupied A site, indicates that the Alu domain will not interfere with a tRNA bound in this position (Fig. 2e, f).

Environment and function of the S domain

The first connection between the S domain and the large ribosomal subunit is formed by the tip of the SRP54 N domain (Fig. 3a). Its two loops, which connect the four-helix bundle, come into close proximity with rpL25 and rpL35 (rpL25/35, corresponding to L23a/L35 in wheat germ and L23p/L29p in *Escherichia coli*). This is in agreement with previous crosslinking experiments identifying the same proteins as the main proteinaceous ribosomal constituents in immediate vicinity to SRP54 (ref. 12). In similar experiments, the same region of the bacterial SRP54 N domain has been found in a position adjacent to L23p[31], suggesting that this interaction is evolutionarily conserved. In addition to SRP, signal sequences[32] and the chaperone trigger factor[33,34] bind to L23p, and the protein-conducting channel (PCC) of the endoplasmic reticulum (the Sec61 complex) binds to rpL25/35 (ref. 20 and Fig. 3g). Thus, the rpL25/35 (L23p/29p) proteins constitute a promiscuous binding site of the ribosome that facilitates interaction with several factors involved in different aspects of cotranslational processing.

The second connection is formed by the N-terminal part of the SRP54 M domain contacting helix 59 (expansion segment 24) of the 25S ribosomal RNA (Fig. 3b, c). As in the first connection involving rpL25/35, this contact site of SRP is shared with the Sec61 complex[20]. The signal sequence is also closest to this connection when bound to SRP in the suggested position.

The third connection engages the C-terminal region of the M domain, in particular the part that binds 7S RNA, which, again like the Sec61 complex, interacts with helix 24 of the 25S ribosomal RNA (Fig. 3b, c). However, in contrast to the Sec61 complex, which contacts the stem of this helix, the SRP-binding site is shifted towards the tip of helix 24. The exclusive involvement of ribosomal RNA in connections 2 and 3 is in agreement with the observation that rpL25/35 (L23p/29p) are the only ribosomal proteins that are crosslinked to SRP54.

Forming the described contacts with the ribosome, SRP54 assumes an open conformation (Fig. 3c, e). How does this relate to the signal-sequence-dependent interaction of SRP with the ribosome? We speculate that in a first step of the ribosome–SRP interaction, which is independent of the signal sequence and involves at least connection 1 (ref. 12), SRP54 switches to a conformation that is competent for signal sequence scanning (sampling mode). In a second step, interaction with a functional signal sequence may induce and stabilize the observed open conformation of SRP54, enabling SRP to bind with high affinity to the ribosome (targeting mode). Notably, the N and the M domains of SRP54 are positioned on the ribosome, thereby determining the orientation of the G domain in between them. As a result, signal sequence binding to the M domain could regulate the nucleotide affinity of the G domain by influencing its position relative to the N domain, which is thought to control nucleotide affinity and GTPase activity[25].

The fourth connection is the only one involving 7S RNA of the S domain (Fig. 3c, d). It seems to be split into two entities, one of which (connection 4a) is very close to helix 5 of SRP; however, it is likely that SRP68/72 is also involved in this connection (4b). The second connection (4b) is located right next to a ribosomal density that has been identified as expansion segment 39 (ref. 22), formed
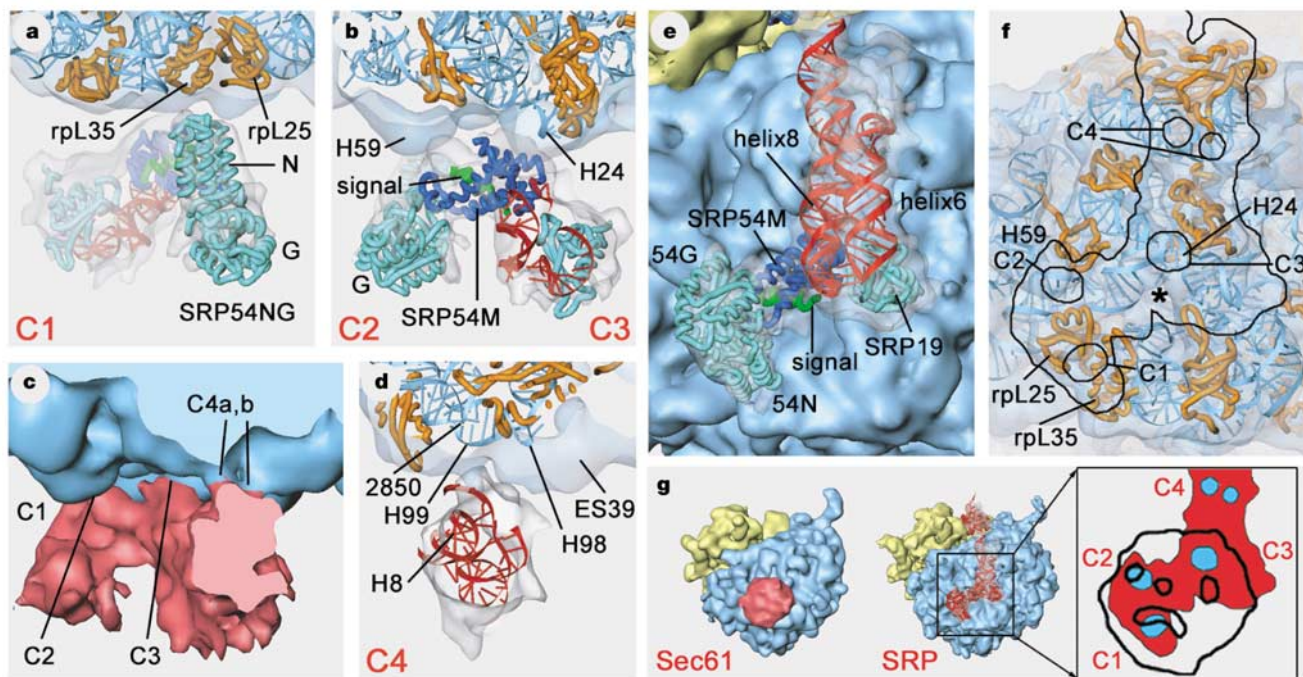
Figure 3 Interaction of the SRP S domain with the 80S ribosome. **a**, Density with molecular models inserted and cut to show connection 1 (C1) between the SRP54 NG domain and rpL25/35. SRP is coloured as in Fig. 2, with 60S ribosomal density and 25S RNA shown in light blue, and 60S proteins in orange. **b**, Connections 2 and 3 (C2, C3) between the SRP54 M domain and ribosomal helices H59 and H24, respectively. **c**, Density in the same orientation as **b** and **d**, cut to show connections C2–C4. **d**, Connection 4 between helix 5 of SRP (and SRP68/72) and the 60S subunit. 2850, position of nucleotide 2,850 in the 25S ribosomal RNA model; H99 and H98, 25S RNA helices; ES39, expansion segment 39. **e**, Model of the S domain covering the peptide exit site of the 60S subunit. **f**, As **e**, with transparent ribosomal density and contour of SRP density showing locations of the connections. Asterisk denotes the peptide tunnel exit. **g**, Comparison of the 80S RNC–Sec61 complex from yeast and the 80S RNC–SRP complex in the same orientation. Magnified area shows the contours of SRP (red) and Sec61 (black line), and their partially overlapping contact sites: SRP (blue), Sec61 (black line).

©2004 **Nature Publishing Group**

by an extension of helix 98 of 25S RNA. In addition, rpL16 (L13p) projects a loop into the vicinity of connection 4. The closest ribosomal structures found for connection 4a are helix 99 and a small loop at the junction between helices 100 and 101 of 25S RNA. Notably, the corresponding region in the *E. coli* ribosome, around nucleotide 2,828 of 23S RNA (nucleotide 2,850 in our model), has been found in the vicinity of bacterial SRP 4.5S RNA by cross-linking[35], again suggesting that there is a conserved mode of interaction.

Thus, considering the previously mentioned localization of SRP54, the core of the eukaryotic S domain, including SRP54 and helices 8 and 5, seems to be positioned on the ribosome in an overall orientation similar to that of its counterpart in prokaryotes.

When comparing the binding sites of SRP and PCC[20,36], it is evident that both cannot bind to the ribosome at the same time (ref. 37 and Fig. 3g). Therefore, docking of the ribosome to the PCC first requires a rearrangement of the whole S domain relative to the ribosome, which is triggered by interaction of the SRP–RNC complex with the SRP receptor[12]. This rearrangement may precede a state in which the binding sites for PCC are accessible and the transfer of the signal sequence can take place.

Environment and function of the Alu domain

The two connections between the Alu domain and the ribosome are contributed exclusively by the 5′ RNP comprising the first 48 nucleotides and the SRP9/14 heterodimer (Fig. 4). In connection 5, the 5′ RNA of the SRP is interacting with both RNA and protein of the large ribosomal subunit (Fig. 4b). Loops L1.2 and L2, as well as the short helix 2 of 7S RNA, contact the large ribosomal subunit through the so-called 'stalk base', and probably through the universally conserved α-sarcin–ricin loop. The participating components of the stalk base are the N-terminal part of rpL12 (L11p) and the tip of helix 43 of 25S ribosomal RNA.

In connection 6, the only contact of SRP with the small ribosomal subunit is established through the SRP9/14 dimer and ribosomal 18S RNA (Fig. 4a). The SRP14 surface mainly participates in contacts with helices 5 and 15 of 18S RNA. SRP9 is in contact with the same helices and, in addition, is close to helix 14. The functionally essential C terminus[38] and a large loop between the β2 and β3 strands of SRP14 are not resolved in the X-ray structure[29]; therefore, at the given resolution we cannot draw any conclusions regarding their participation in ribosomal contacts.

The ribosomal components bound by the Alu domain are well conserved in all ribosomes and comprise the elongation-factor-binding site[39]. It is intriguing that all of the contact sites used by the SRP Alu domain are also used by eEF2 (refs 40, 41), enabling us to interpret the Alu–ribosome interaction as elongation factor mimicry (Fig. 4c). A tRNA-like interaction, however, takes place concomitantly: the RNA–RNA interaction between loop L2 of the SRP 5′ RNP and helix 43 of the stalk base is reminiscent of the interaction between the tRNA T-loop and the same ribosomal helix in the context of the EF-Tu–tRNA–GTP ternary complex bound to the ribosome[42].

Binding of the Alu domain in this position directly competes with elongation factors entering their binding site (Fig. 4c). Therefore, sufficiently high affinity of the Alu domain for this site explains its elongation arrest activity. Variations in Alu-domain affinity could explain the different efficiencies observed in different systems[16,43]. In our structure, the Alu domain is bound to a ribosome in the post-translocational conformation ('post' state), as defined by the presence of the peptidyl-tRNA in the P site and an unoccupied A site. Thus, it is possible that the post state of the ribosome is the preferred
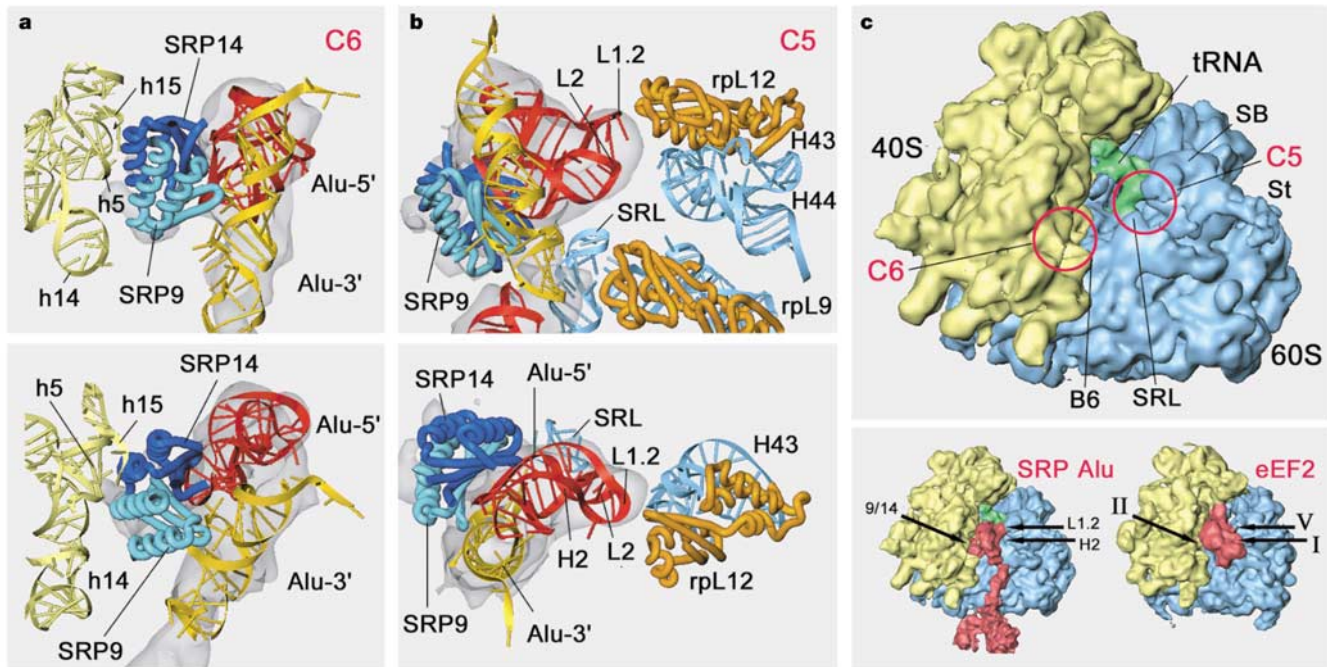
Figure 4 Interaction of the SRP Alu domain with the 80S ribosome. **a**, Top, SRP density with models showing connection 6 (C6) between SRP9/14 and ribosomal 18S RNA (helices 5, 15 and 14) in an orientation similar to Fig. 1b. Colour coding is the same as in Figs 2 and 3, with 18S ribosomal RNA shown in pale yellow. Bottom, as top view, but tilted towards the viewer. **b**, Top, connection 5 (C5) between SRP Alu RNA (loop 1.2 and helix 2) and the GAC of the 60S ribosomal subunit (rpL12, helix 43 and the α-sarcin–ricin loop (SRL)). Bottom, as top view, but tilted towards the viewer. **c**, Top, 80S RNC density without SRP, showing conserved contact sites of the Alu domain. B6, bridge 6. Bottom, comparison of the 80S RNC–SRP complex and the 80S ribosome–eEF2 complex[41] in the same orientation (SRP and eEF2 are shown in red). Subunits of the Alu domain and domains of eEF2 involved in similar contact sites are labelled.
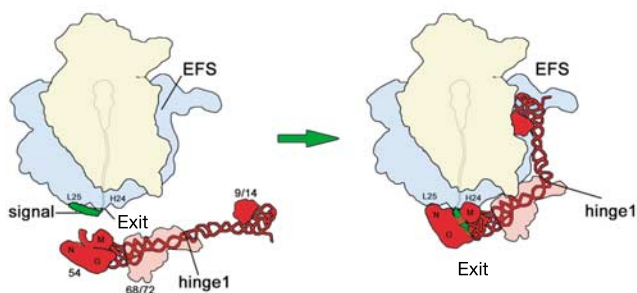
Figure 5 Signal-sequence-dependent SRP–ribosome interaction. On signal sequence binding by SRP54, a kinked conformation of SRP involving possibly SRP68/72 and a rotation around hinge 1 is stabilized. As a result, SRP interacts with the ribosome, stretching from the peptide exit (S domain) to the elongation-factor-binding site in the intersubunit space (Alu domain), where it causes elongation arrest by competition with elongation factors. Colour coding is the same as in Fig. 1, with the signal sequence (signal) shown in green. Exit, peptide tunnel exit; EFS, elongation-factor-binding site.

conformation for SRP binding during the elongation cycle[44].

How can elongation arrest by the Alu domain be controlled by the event of signal sequence binding, which occurs more than 250 Å away? Signal sequence binding has to induce or at least to stabilize bending[45] of the particle at hinge 1 to promote Alu-domain binding (Fig. 5). One possibility is that high-affinity binding of the S domain simply tethers the Alu domain in an appropriate position on the ribosome, and thereby favours the bound-state conformation of SRP. However, we prefer another model in which the recognition of a signal peptide produces specific positioning of the S domain on the ribosome; this may lead to conformational changes in SRP68/72 that result in hinge 1 stabilizing a 90° angle and the Alu domain closing into the elongation-factor-binding site (Fig. 5). In agreement with this idea is the brace-like localization of SRP68/72 covering the hinge 1 region, its participation in connection 4, and the finding that SRP reconstituted without SRP68/72 lacks elongation arrest activity[17].

Conclusions

The structure of the eukaryotic SRP–RNC targeting complex shows that SRP accomplishes its task of signal sequence recognition and elongation pausing by spanning from the peptide exit site to the elongation-factor-binding site of the ribosome in a kinked conformation. The ribosomal contacts involve 7S RNA and all SRP proteins, with the exception of SRP19. SRP54, as the main protagonist of the S domain, establishes an open conformation directly across the peptide exit site and SRP68/72 may communicate between the S and the Alu domains. The position of the Alu domain in the elongation-factor-binding site explains its elongation arrest activity by direct competition. The structure suggests that the conserved core of the S domain of SRP is likely to follow the same mode of ribosome interaction and functioning in all organisms. □

Methods

Purification of RNCs

To generate purified RNCs, we used a wheat germ *in vitro* translation system (Ambion) programmed with truncated mRNA encoding the 90 N-terminal amino acids of DPAP-B from *Saccharomyces cerevisiae*. Purification was done by a modified protocol[20]. A DNA fragment with N-terminal histidine and HA tags was generated by polymerase chain reaction from yeast genomic DNA using forward (5′-taatacgactcactatagggaccaaa caaaacaaataaaacaaaaacacaatgtctcatcatcatcatcatcattacccatagatgttccagattacgctgaaggtggcgaag aagaagttg-3′) and reverse (5′-ttgcagctcgtgatatttgggatg-3′) primers. We then synthesized capped mRNA by a Message Machine kit (Ambion). For translation, six 200-µl reactions were incubated for 45 min at 27 °C and terminated with 2 µl of 10 mg ml⁻¹ cycloheximide.

Reactions were spun through a high-salt sucrose cushion (50 mM Tris-HCl (pH 7.0), 500 mM potassium acetate, 25 mM magnesium acetate, 2 mM dithiothreitol (DTT), 1 M sucrose and 10 µg ml⁻¹ cycloheximide) at 355,000*g* for 45 min. Pellets were resuspended in ice-cold 250 buffer (50 mM Tris-HCl (pH 7.0), 250 mM potassium acetate, 25 mM

magnesium acetate, 0.1% (w/v) Nikkol, 5 mM β-mercaptoethanol, 10 µg ml⁻¹ cycloheximide and 250 mM sucrose) and transferred to 1.5 ml of Talon metal-affinity resin (Clontech). The resin was washed with 8 ml of 250 buffer, and 2 ml of 500 buffer (250 buffer containing 500 mM potassium acetate). RNCs were eluted with 100 mM imidazol (pH 7.1) in 250 buffer and spun through 500 µl of a high-salt sucrose cushion. The resulting pellet was slowly resuspended in G buffer (20 mM Tris-HCl (pH 7.0), 50 mM potassium acetate, 10 mM magnesium acetate, 1 mM DTT, 125 mM sucrose, 100 µg ml⁻¹ cycloheximide, 0.05% (w/v) Nikkol and 0.03% (w/v) of an EDTA-free complete protease inhibitor pill (Boehringer) and 0.2 U µl⁻¹ RNasin (Ambion)), flash frozen and stored at −80 °C. From 1.2 ml of translation reaction, RNCs with an absorbance of 0.7 at 260 nm (~15 pmol) were isolated.

Reconstitution of the SRP–RNC complex

RNC–SRP complexes were reconstituted by incubating 1.5 pmol of mammalian SRP (isolated as described[46] and further purified by sucrose density gradient centrifugation[47]) and 0.5 pmol of RNCs for 15 min at room temperature in 25 mM HEPES (pH 7.5), 150 mM potassium acetate, 5 mM DTT, 5 mM magnesium acetate, 100 mM sucrose, 0.02% Nikkol, 100 µg ml⁻¹ cycloheximide and 0.06% of an EDTA-free complete protease inhibitor pill. The reaction was spun through a 10–40% high-salt sucrose cushion (500 mM potassium acetate) and analysed by SDS–PAGE. For cryo-EM, 1 pmol of RNCs was incubated with 3 pmol of SRP in a volume of 28 µl under the described conditions, except that the potassium acetate concentration was 180 mM.

Electron microscopy, image processing and models

Samples were applied to carbon-coated holey grids as described[48]. Micrographs were recorded under low-dose conditions on a Tecnai F30 field emission gun electron microscope at 300 kV and a Tecnai F20 instrument at 160 kV in a defocus range of 1.0 µm to 4.5 µm, and scanned on a Heidelberg drum scanner, resulting in a pixel size of 3.26 Å on the object scale. The data were analysed by the SPIDER software package. After automated particle picking followed by visual inspection, 35,488 particles were selected for density reconstruction. We sorted the data set into subsets (±SRP) according to a procedure developed by C.M.T.S., P. Penczek and J.F. (unpublished). Removal of particles lacking the SRP resulted in two subsets of 10,091 (−SRP) and 25,397 (+SRP) particles, which were used for the final CTF-corrected reconstruction at a resolution of 12.0 Å (7.7 Å), based on the Fourier shell correlation with a cutoff value of 0.5 (3σ). Densities for the 40S subunit, the 60S subunit, the P-site tRNA and the SRP were isolated by using binary masks. Amplitude correction was done by Fourier filtering using *B* factors. A lower contour level of the SRP density for surface representation was applied. This indicates that the SRP density is under-represented because of incomplete removal of SRP-free ribosomal particles from the final particle subset (the same contour level is shown in Supplementary Fig. 1).

Docking of X-ray structures and molecular models of SRP was done by the programs SPIDER and O[49]. First, a fragment of the mammalian S domain containing 7S RNA helices 6–8, part of helix 5, SRP19 and the SRP54 M domain (Protein Data Bank (PDB) accession code 1MFQ; ref. 23) was docked. The M domain was replaced by a different model[24] using the RNA-binding moiety for alignment. The structure of a prokaryotic SRP54 NG domain (PDB 1JPJ; ref. 25) was docked into density present near the M domain. An α-helical peptide fragment was docked as the signal sequence. The X-ray structure of the mammalian Alu 5′ RNP (PDB 1E8O; ref. 29) was docked and, for the missing part of the 7S RNA, three fragments were used from a model provided by the SRP database[30]. The high degree of similarity between the wheat germ and the yeast RNC allowed us to use a molecular model of the yeast ribosome (PDB 1K5X, 1K5Y and 1K5Z; ref. 22). The figures were prepared by using Iris Explorer (NAG), Ribbons[50] and POV-Ray.

1. Blobel, G. & Sabatini, D. in *Biomembranes* (ed. Manson, L. A.) 193–195 (Plenum, New York, 1971).
2. Walter, P., Ibrahimi, I. & Blobel, G. Translocation of proteins across the endoplasmic reticulum. I. Signal recognition protein (SRP) binds to *in-vitro*-assembled polysomes synthesizing secretory protein. *J. Cell Biol.* **91,** 545–550 (1981).
3. Koch, H. G., Moser, M. & Muller, M. Signal recognition particle-dependent protein targeting, universal to all kingdoms of life. *Rev. Physiol. Biochem. Pharmacol.* **146,** 55–94 (2003).
4. Gundelfinger, E. D., Krause, E., Melli, M. & Dobberstein, B. The organization of the 7SL RNA in the signal recognition particle. *Nucleic Acids Res.* **11,** 7363–7374 (1983).
5. Siegel, V. & Walter, P. Each of the activities of signal recognition particle (SRP) is contained within a distinct domain: analysis of biochemical mutants of SRP. *Cell* **52,** 39–49 (1988).
6. Walter, P. & Blobel, G. Disassembly and reconstitution of signal recognition particle. *Cell* **34,** 525–533 (1983).
7. Connolly, T. & Gilmore, R. The signal recognition particle receptor mediates the GTP-dependent displacement of SRP from the signal sequence of the nascent polypeptide. *Cell* **57,** 599–610 (1989).
8. Bernstein, H. D. *et al.* Model for signal sequence recognition from amino-acid sequence of 54K subunit of signal recognition particle. *Nature* **340,** 482–486 (1989).
9. Romisch, K., Webb, J., Lingelbach, K., Gausepohl, H. & Dobberstein, B. The 54-kD protein of signal recognition particle contains a methionine-rich RNA binding domain. *J. Cell Biol.* **111,** 1793–1802 (1990).
10. Batey, R. T., Rambo, R. P., Lucast, L., Rha, B. & Doudna, J. A. Crystal structure of the ribonucleoprotein core of the signal recognition particle. *Science* **287,** 1232–1239 (2000).
11. Zopf, D., Bernstein, H. D., Johnson, A. E. & Walter, P. The methionine-rich domain of the 54 kD protein subunit of the signal recognition particle contains an RNA binding site and can be crosslinked to a signal sequence. *EMBO J.* **9,** 4511–4517 (1990).
12. Pool, M. R., Stumm, J., Fulga, T. A., Sinning, I. & Dobberstein, B. Distinct modes of signal recognition particle interaction with the ribosome. *Science* **297,** 1345–1348 (2002).
13. Siegel, V. & Walter, P. Removal of the Alu structural domain from signal recognition particle leaves its

protein translocation activity intact. *Nature* **320,** 81–84 (1986).

14. Walter, P. & Blobel, G. Translocation of proteins across the endoplasmic reticulum. III. Signal recognition protein (SRP) causes signal sequence-dependent and site-specific arrest of chain elongation that is released by microsomal membranes. *J. Cell Biol.* **91,** 557–561 (1981).

15. Wolin, S. L. & Walter, P. Signal recognition particle mediates a transient elongation arrest of preprolactin in reticulocyte lysate. *J. Cell Biol.* **109,** 2617–2622 (1989).

16. Mason, N., Ciufo, L. F. & Brown, J. D. Elongation arrest is a physiologically important function of signal recognition particle. *EMBO J.* **19,** 4164–4174 (2000).

17. Siegel, V. & Walter, P. Elongation arrest is not a prerequisite for secretory protein translocation across the microsomal membrane. *J. Cell Biol.* **100,** 1913–1921 (1985).

18. Andrews, D. W., Walter, P. & Ottensmeyer, F. P. Evidence for an extended 7SL RNA structure in the signal recognition particle. *EMBO J.* **6,** 3471–3477 (1987).

19. Nagai, K. *et al.* Structure, function and evolution of the signal recognition particle. *EMBO J.* **22,** 3479–3485 (2003).

20. Beckmann, R. *et al.* Architecture of the protein-conducting channel associated with the translating 80S ribosome. *Cell* **107,** 361–372 (2001).

21. Walter, P. & Blobel, G. Subcellular distribution of signal recognition particle and 7SL-RNA determined with polypeptide-specific antibodies and complementary DNA probe. *J. Cell Biol.* **97,** 1693–1699 (1983).

22. Spahn, C. M. *et al.* Structure of the 80S ribosome from *Saccharomyces cerevisiae* tRNA–ribosome and subunit–subunit interactions. *Cell* **107,** 373–386 (2001).

23. Kuglstatter, A., Oubridge, C. & Nagai, K. Induced structural changes of 7SL RNA during the assembly of human signal recognition particle. *Nature Struct. Biol.* **9,** 740–744 (2002).

24. Huang, Q., Abdulrahman, S., Yin, J. & Zwieb, C. Systematic site-directed mutagenesis of human protein SRP54 in signal recognition particle RNA and modes of signal peptide recognition. *Biochemistry* **41,** 11362–11371 (2002).

25. Padmanabhan, S. & Freymann, D. M. The conformation of bound GMPPNP suggests a mechanism for gating the active site of the SRP GTPase. *Struct. Fold. Des.* **9,** 859–867 (2001).

26. Rosendal, K. R., Wild, K., Montoya, G. & Sinning, I. Crystal structure of the complete core of archaeal signal recognition particle and implications for interdomain communication. *Proc. Natl Acad. Sci. USA* **100,** 14701–14706 (2003).

27. Siegel, V. & Walter, P. Binding sites of the 19-kDa and 68/72-kDa signal recognition particle (SRP) proteins on SRP RNA as determined in protein–RNA 'footprinting'. *Proc. Natl Acad. Sci. USA* **85,** 1801–1805 (1988).

28. Ban, N., Nissen, P., Hansen, J., Moore, P. B. & Steitz, T. A. The complete atomic structure of the large ribosomal subunit at 2.4 Å resolution. *Science* **289,** 905–920 (2000).

29. Weichenrieder, O., Wild, K., Strub, K. & Cusack, S. Structure and assembly of the Alu domain of the mammalian signal recognition particle. *Nature* **408,** 167–173 (2000).

30. Rosenblad, M. A., Gorodkin, J., Knudsen, B., Zwieb, C. & Samuelsson, T. SRPDB: signal recognition particle database. *Nucleic Acids Res.* **31,** 363–364 (2003).

31. Gu, S. Q., Peske, F., Wieden, H. J., Rodnina, M. V. & Wintermeyer, W. The signal recognition particle binds to protein L23 at the peptide exit of the *Escherichia coli* ribosome. *RNA* **9,** 566–573 (2003).

32. Eisner, G., Koch, H. G., Beck, K., Brunner, J. & Muller, M. Ligand crowding at a nascent signal sequence. *J. Cell Biol.* **163,** 35–44 (2003).

33. Kramer, G. *et al.* L23 protein functions as a chaperone docking site on the ribosome. *Nature* **419,** 171–174 (2002).

34. Ullers, R. S. *et al.* Interplay of signal recognition particle and trigger factor at L23 near the nascent chain exit site on the *Escherichia coli* ribosome. *J. Cell Biol.* **161,** 679–684 (2003).

35. Rinke-Appel, J. *et al.* Crosslinking of 4.5S RNA to the *Escherichia coli* ribosome in the presence or absence of the protein Ffh. *RNA* **8,** 612–625 (2002).

36. Morgan, D. G., Menetret, J. F., Neuhof, A., Rapoport, T. A. & Akey, C. W. Structure of the mammalian ribosome–channel complex at 17 Å resolution. *J. Mol. Biol.* **324,** 871–886 (2002).

37. Moller, I. *et al.* A general mechanism for regulation of access to the translocon: competition for a membrane attachment site on ribosomes. *Proc. Natl Acad. Sci. USA* **95,** 13425–13430 (1998).

38. Thomas, Y., Bui, N. & Strub, K. A truncation in the 14 kDa protein of the signal recognition particle leads to tertiary structure changes in the RNA and abolishes the elongation arrest activity of the particle. *Nucleic Acids Res.* **25,** 1920–1929 (1997).

39. Wilson, D. N. *et al.* Protein synthesis at atomic resolution: mechanistics of translation in the light of highly resolved structures for the ribosome. *Curr. Protein Peptide Sci.* **3,** 1–53 (2002).

40. Gomez-Lorenzo, M. G. *et al.* Three-dimensional cryo-electron microscopy localization of EF2 in the *Saccharomyces cerevisiae* 80S ribosome at 17.5 Å resolution. *EMBO J.* **19,** 2710–2718 (2000).

41. Spahn, C. *et al.* Domain movements of elongation factor eEF2 and the eukaryotic 80S ribosome facilitate tRNA translocation. *EMBO J.* (in the press).

42. Valle, M. *et al.* Incorporation of aminoacyl-tRNA into the ribosome as seen by cryo-electron microscopy. *Nature Struct. Biol.* **10,** 899–906 (2003).

43. Wolin, S. L. & Walter, P. Ribosome pausing and stacking during translation of a eukaryotic mRNA. *EMBO J.* **7,** 3559–3569 (1988).

44. Ogg, S. C. & Walter, P. SRP samples nascent chains for the presence of signal sequences by interacting with ribosomes at a discrete step during translation elongation. *Cell* **81,** 1075–1084 (1995).

45. Andreazzoli, M. & Gerbi, S. A. Changes in 7SL RNA conformation during the signal recognition particle cycle. *EMBO J.* **10,** 767–777 (1991).

46. Martoglio, B., Hauser, S. & Dobberstein, B. in *Cell Biology: A Laboratory Handbook* (ed. Celis, J. C.) 265–273 (Academic, San Diego, 1997).

47. Walter, P. & Blobel, G. Signal recognition particle: a ribonucleoprotein required for cotranslational translocation of proteins, isolation and properties. *Methods Enzymol.* **96,** 682–691 (1983).

48. Wagenknecht, T., Grassucci, R. & Frank, J. Electron microscopy and computer image averaging of ice-embedded large ribosomal subunits from *Escherichia coli*. *J. Mol. Biol.* **199,** 137–147 (1988).

49. Jones, T. A., Zhou, J. Y., Cowan, S. W. & Kjeldgaard, M. Improved methods for building protein models in electron density maps and the location of errors in these models. *Acta Crystallogr. A* **47,** 110–119 (1991).

50. Carson, M. Ribbons 2.0. *Appl. Crystallogr.* **24,** 103–106 (1991).